First-principles studies of the Optical anisotropy of $R3$(No.146) space group chalcogenides crystal AX_2MQ_6

Jusong Yu*

University of Chinese Academy of Sciences, Beijing 100039, People's Republic of China
js.yu@fjirsm.ac.cn

Hua Lin†

Fujian Institute of Research on the Structure of Matter, CAS, Fuzhou, Fujian 350002, People's Republic of China
linhua@fjirsm.ac.cn

liming Wu‡

Fujian Institute of Research on the Structure of Matter, CAS, Fuzhou, Fujian 350002, People's Republic of China
limingwu@fjirsm.ac.cn

November 10, 2018

Abstract

The birefringence values of R3(No.146) space group crystals AX_2MQ_6 have been calculated. Their Electron Localization Function(ELF) was calculated to show that the acentricity of the bonds on sp^3 hybridization Q^{2-} ions is the main origin of optical anisotropy. To quantificat the acentricity, a geometric parameter dihedral angle between tetrahedral undersides and xy-planes was defined. We find theoretically the birefringence depend on the defined geometric parameter and ion radius. This relation between birefringence and structure can be used to explain the abnormal difference of birefringence of isostructural AX_2MQ_6 and $AX_4M_5Q_{12}$ and useful for exploring new phase matching IR-NLO crystal.

I. TOC

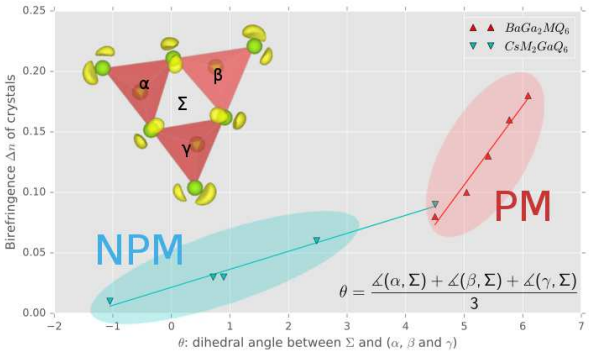

II. Introduction

IR-NLO materials contain the following conditions will have potential applicability:

- Large second nonlinear optical susceptibility χ for a IR-NLO crystal which should be at least 10 times (preferably 20 times) larger than that of KDP ($d_{max} = 0.39\,\mathrm{pm}$).[1]
- An moderate birefringence and linear optical dispersion which make the crystal phase-matched in the condition is necessary.[2] The approprate birefringence should be large enough to achieve the phase-matching in the IR region but not too large to generate considerable self-focus[3] and walk-off effects[4].
- Large band gap E_g for high laser damage threshold[5].

*A thank you or further information
†Corresponding author
‡Corresponding author

The $AX_4M_5Q_{12}$[6] synthesised by H Lin *et al.* have strong NLO response (roughly 16-40 times that of commercial $AgGaS_2$) at IR range. However, the birefringence of these compounds come near to zero which means they are close to isotropic crystal which are impossible to reach type I phase matching. On the contrary, the $BaGa_2SnSe_6$[7] synthesised by X Li *et al.* have extremly large birefringence values and exhibits very strong NLO response(5.2 times that of the benchmark $AgGaS_2$ at the laser frequency 2.09 µm). There are some symmorphic structures $BaGa_2MQ_6$[8] (M = Si, Ge; Q = S, Se) published by W Yin *et al.* and $CsSn_2XSe_6$ (X = In, Ga) phblished by H Lin *et al.* exhibits moderate birefringence and large bandgaps.

The AX_2MQ_6 and $AX_4M_5Q_{12}$ have the similar structure which belongs to *R*3(No.146) space group and can be derived from the zinc-blende structure so that we call them the diamond-like framework structure(DLF)[9]. The two similar structure show the entirely different anisotropic properties. The birefringence value of $AX_4M_5Q_{12}$ is very small (<0.01) while AX_2MQ_6 have a wide range birefringence (0.006 to 0.186) in trasmission wavelengths[6].

In transparent materials, refractive index is proportional to the square root of the electronic polarization. The latter is in turn proportional to the polarizabilities of the ions in the crystal and also the local electric field.[10] And optical anisotropy gives rise to the phenomenon of birefringence.[11] We can calculate the values of refractive index by using ab initio and empirical (or semiempirical) methods[12,13]. The ab initio method is difficult to construct explicit structural-properties relation though it can be taken to make precise values of refractive index. As for empirical(or semiempirical) methods, they only calculated the mean refractive indices without consideration of birefringence.

The refractive indices of materials strongly relate to the space strucure. Densely packed arrays of highly polarizable groups result in large refractive indices. And the different direction of polarizable groups lead to the different refractive indices of ordinary and extraordinary optical planes which is the reason of birefringence of crystals[10]. The structural-birefringence relationship is revealed in some 0D inorganic borate materials[14,15]. These borate materials are constructed by isolated B−O groups which is the dominating factors of anisotropy so that the packed mode can be easily described to relate birefringence. However, AX_2MQ_6 and $AX_4M_5Q_{12}$ are 3D inoganic crystals which are hard to attribute the optical anisotropy to isolate groups or molecules.

In our work, we develop a resonable way to deal with site partial occupation in these structure. Then conclude $CsSn_2GaSe$ and five existent BaGa2XQ6 compounds which have different birefrigence and nonlinear optical susceptibility to reveal the dependence on the ion radius and the defined geometric parameters of birefringence. Derived from these six isosymophic compounds, we construct four hypothetic compounds CsM_2GaQ_6(M=Si,Ge; Q=S,Se) to confirm the defined geometric parameters dependence. The Electron Localization Function(ELF)[16] was represented to explain the reason why we defined the dihedral angle between tetrahedral undersides and xy-planes and show the relation of structure and optical anisotropy.

III. Computational Method

To deal with the fractional site occupation uncertainty in AX_2MQ_6, the twelve initial geometries of structures represented in a hexagonal conventional cell was enumerated by using SOD(site-occupancy disorder) program[17]. The DFT and optical property calculations in the study were performed using the Quantum-Espresso(QE)[18] and Vienna Ab initio Simulation Package (VASP)[19].

Geometries relaxiation were performed in QE optimized using PBEsol[20] GGA with pz-LDA and PBE as comparison. Electronic wave functions (density) were expanded in plane waves up to 40Ry (320Ry) and ultrasoft pseudopotential (rrkjus) was used to treat valence electrons. Pseudovalence electronic configurations were Cs: $6s^1$, Ba: $5s^25p^65s^2$, Cd: $4d^{9.5}5s^25p^{0.5}$, Ga: $3d^{10}4s^24p^1$, In: $4d^{10}5s^25p^1$, Sn: $4d^{10}5s^25p^2$, Si: $3s^23p^23d^{-2}4f^{-2}$, Ge: $3d^{10}4^s24p^2$, Se: $3d^{10}4s^24p^44d^{-2}$ and S: $3s^23p^43d^{-2}$. Monkhorst-Pack (MP)[21] k-point meshes were used for the Brillouin zone (BZ) integrations and convergence was tested to zone-edge-shifted $4 \times 4 \times 4$. During structure relaxiation, the forces were converged to values of less than 0.001 a.u.

In the linear optical properties calculation done with VASP, a projector-augmented plane-wave method[22], with 600-eV energy cutoff was utilized and with the electronic configuration for the involved elements: Cs: $5s^25p^66s^1$, Ba: $5s^25p^66s^2$, Cd: $5s^24d^{10}$, Ga: $4s^24p^1$, In: $5s^25p^1$, Sn: $5s^25p^2$, Si: $3s^23p^2$, Ge: $3d^{10}4s^24p^2$, Se: $4s^24p^4$ S: $3s^23p^4$. To get resonable optical properties, brillouin zone sampling meshes were increased and tested to convergence to $9 \times 9 \times 9$ with none-shifted Monkhorst-Pack (MP) method.

(a) Rhombohedral setting

(b) Hexagonal setting

Figure 1 Two settings for AX_2MQ_6 crystals

VASP calculates the frequency dependent dielectric matrix after the electronic ground state has been determined. The imaginary part is determined by a summation over empty states using the equation[23]:

$$\varepsilon^{(2)}_{\alpha\beta}(\omega) = \frac{4\pi^2 e^2}{\Omega} \times \lim_{q\to 0} \frac{1}{q^2} \sum_{c,v,k} 2w_k \delta(\epsilon_c k - \epsilon_v k - \omega) \times \langle u_{ck+e_{\alpha q}} | u_{vk} \rangle \langle u_{ck+e_{\alpha q}} | u_{vk} \rangle^* \quad (1)$$

where the indices c and v refer to conduction and valence band states respectively, and $u_{c\mathbf{k}}$ is the cell periodic part of the orbitals at the k-point $\mathbf{k}$. This method is performed without containing the local-Field effects[24] and excitonic effects[25].

The real part of the dielectric tensor $\varepsilon^{(1)}$ is obtained by the usual Kramers-Kronig transformation

$$\varepsilon^{(1)}_{\alpha\beta}(\omega) = 1 + \frac{2}{\pi} P \int_0^\infty \frac{\varepsilon^{(2)}_{\alpha\beta}(\omega')\omega'}{\omega'^2 - \omega^2 + i\eta} d\omega' \quad (2)$$

where P denotes the principle value.

The static second-order susceptibility, $\chi^{(2)}$, is important for characterizing the NLO properties. The crystal orbital or band structure methods to calculate the NLO coefficients have been greatly improved and successfully used to predict the SHG coefficients for semiconductors and insulators. The length-gauge formalism derived by Aversa and Sipe[26] and modified by Rashkeev *et al.*[27] is adopted in our calculation. The imaginary part of the static second-order optical susceptibility can be expressed as:

$$\begin{aligned} \chi^{abc} &= \chi^{abc}_e + \chi^{abc}_i \\ &\frac{e^3}{\hbar\Omega} \sum_{nml,k} \frac{r^a_{nm}\{r^b_{ml} r^c_{ln}\}}{\omega_{nm}\omega_{ml}\omega_{ln}} [\omega_n f_{ml} + \omega_m f_{ln} + \omega_l f_{nm}] \\ &+ \frac{i}{4}\frac{e^3}{\hbar\Omega} \sum_{nm,k} \frac{f_{nm}}{\omega^2_{mn}} [r^a_{nm}(r^b_{mn;c} + r^c_{mn;b}) \\ &+ r^b_{nm}(r^a_{mn;c} + r^c_{mn;a}) + r^c_{nm}(r^a_{mn;b} + r^b_{mn;a})]. \end{aligned} \quad (3)$$

IV. Results and discussion

i. Structure and Electronic Structure

The AX_2MQ_6 belong to trigonal crystal system and have R3(No.146) space group symmetry with A=Cs, Ba; Q=S, Se. To balance the valence, X and M are 3+ and 4+ respectively for A=Ba or X=X^{4+} and M=M^{3+} if A = Cs. There are two ways to represent R3 space group crystal, in hexagonal setting Fig.1b or Rhombohedral setting 1a.[28]

Taking BaX2MQ6 as object of study and representing by using rhombohedral setting, the unit cell contains 10 atoms that Ba ion on vertex and three $[(X/M)Q_4]^{n-}$ tetrahedral anions. Fig.1a The structural analysis reveals that X and M ramdonly occupy the same Wickoff site 3b with the ratio of X:M=2:1[8]. Viewed from the screw 3_1-axis, xy-planes are tiled by the bundles of three tetrahedrons shown in Fig.**??**. This kind of relatively dispersive occupation of tetrahedral bundles potentially influence the freedom of tetrahedral polarizable directions which lead to the different birefringence of AX_2MQ_6 as we will discuss later.

In order to proper deal with the DFT calculation, we are going to choose one complete occupation configuration by using SOD program. Instead of extending

$BaGa_2SiS_6$	a	c	V
exp	9.5544(2)	8.6498(4)	683.82(2)
PBEsol	9.462	8.556	663.318
$BaGa_2SiSe_6$	a	c	V
exp	9.967(1)	9.047(2)	778.3(2)
PBEsol	9.925	9.006	768.225
$BaGa_2GeS_6$	a	c	V
exp	9.6020(1)	8.6889(2)	693.78(2)
PBEsol	9.502	8.623	674.275
$BaGa_2GeSe_6$	a	c	V
exp	10.008(1)	9.090(2)	788.4(2)
PBEsol	9.949	9.093	779.410
$BaGa_2SnSe_6$	a	c	V
exp	10.1449(14)	9.2490(18)	824.4
PBEsol	10.054	9.326	816.477

Table 1 Lattice parameters compare with experiment data

the rhombohedral primitive cell to supercell and collect different models, we adopt hexagonal axes representation which is three times larger in cell volume of the rhombohedral primitive cell. Consquently, we enumerate all twelve nonequivalent configurations from a 1x1x1 hexagonal primitive cell as list in SI fig*. After analyse symmetry of twelve configurations, we get nine $P1$(No.1) space group configurations and three configurations whose space group are $P3_2$(No.145), $P3_1$(No.144) and $P3$(No.143) respctively which are subgroups of $R3$(No.146). To conform with the X-ray diffraction experiment results that the lattice parameters a and b in the conventional cell are equal, we excluded nine P1 configurations and compare the ground state energy of the relaxed $P3$, $P3_1$, $P3_2$ configurations to choose the most resonable object for the subsequent study.

Three configurations $P3_2$(No.145), $P3_1$(No.144) and $P3$(No.143) of each $BaGa_2MQ_6$ compound is relax to optimal structure and then the groud state energy is extracted. Three kinds of DFT exchange-correlate energy are employed: (1) using LDA (2) using PBE and (3) using PBEsol. Results are summarised in Table.4. It shows PBEsol can precisively describe the ground state structure of $BaGa_2MQ_6$. From Table.5 we can find that $P3_2$ and $P3_1$ configurations always have lower energy than $P3$ configurations, which means the model of these two configurations are more closely similar to the real crystal structures.

We conclude from the data that the more dispersive the occupied atom species are, the lower the groud state energy are. The $P3_1$(No.144) model relaxed by using PBEsol is suitable as the object to continue the properties calculation. Therefore we take the $P3_1$(No.144) configuration with PBEsol relaxed structure as the model for subsquent property studies.

The band structures are shown in Fig[] in the Supporting Information. From the band structure, we find all AX_2MQ_6 are indirect band crystal with calculated band gap range from 1.332eV to 3.078eV for $CsGa_2SnSe_6$ to CsSi2GaS6. The values of band gap are decrease with the atomic number. Analysis of the partail density of states (PDOS) (Table.**??**) show that A^{n+} cations mainly occuppied the energy far below the fermi energy. The transition from occupied states to unoccupied states are mainly determinated by Q^{2-} atoms. And this is the reason of subsequent analysis of birefringence that we focus on the acentricity of the sp^3 hybridization Q^{2-} ions.

ii. Stability of hypothetical $CsGaM_2Q_6$

Up to now, five kinds of $BaGa_2MQ_6$ with M=Si,Ge,Sn; Q=S,Se, $CsGaSn_2Se$ and $CsInSn_2Se$ have been synthesized, which can be taken as indication of the stabilities of the derived hypothetical crystals $CsGaM_2Q_6$ with M=Si,Ge and Q=S,Se. We calculated the cohesive energies of AX_2MQ_6, which is defined as the energy required to form separated neutral atoms in their ground electronic state from the state at 0K and 1atm.[] Cohesive energies of AX_2MQ_6 are obtained using the expression:

$$E_C = \{\sum_n p_n E_c[n] - E_t[Crystal]\} / \sum p_n \qquad (4)$$

n is the atom species of crystal.

The calculated cohesive energies of seven existent structure and four deuterogenic structure CsM_2GaQ_6 are given in Table.2. We note that even CsM_2GaQ_6 (M= Si,Ge; Q= S, Se) are not synthesised yet, they are more cohesive energy stable.

iii. Linear Optical properties of AX2MQ6 crystals

The model we adopt to calculate the optical properties are the $R3$ (No.144) space group configuration and its point group is C_3 which belongs to the uniaxial crystal classes. Therefore only two independent dielectric constant ϵ_{xy}(in plane component the average over the x and the y directions) and ϵ_z(z component perpendicular to ϵ_{xy}) will appear in the results.

In synthetic chemistry, phase matching ability is tested by using the Kurtz-Perry powder[29] method (without

Table 2 Cohesive energies E_C of AGa_2QM_6 crystals.

Structure	$E_c \times \sum p_n$(eV)	Structure	E_c(eV)
$BaGa_2SiS_6$	119.923	$CsSi_2GaS_6$	116.981
$BaGa_2SiSe_6$	107.812	$CsSi_2GaSe_6$	104.288
$BaGa_2GeS_6$	114.790	$CsGe_2GaS_6$	106.897
$BaGa_2GeSe_6$	103.834	$CsGe_2GaSe_6$	96.689
$BaGa_2SnSe_6$	102.515	$CsSn_2GaSe_6$	94.356

needs of sigle crystals). These are type-I phase matching case in which the two lower-frequency waves have the same polarization[30 4].

In positive uniaxial crystal and for the type I phase matching the condition is:

$$\begin{aligned} n_e^{\nu} &> n_o^{2\nu} \qquad \text{or} \\ n_e^{2\nu} - n_o^{2\nu} &> n_e^{2\nu} - n_e^{\nu} \end{aligned} \tag{5}$$

which is different from the type I negtive uniaxial crystall phase matching condition:

$$\begin{aligned} n_o^{\nu} &> n_e^{2\nu} \qquad \text{or} \\ n_o^{2\nu} - n_e^{2\nu} &> n_o^{2\nu} - n_o^{\nu} \end{aligned} \tag{6}$$

Both expressions 5 and 6 for negtive and positive uniaxial crystals show that if birefrigence in frequency 2ν is larger, the phase matching condition is more possible to be achieved (exceptional case may result from intensity depend index of refractive[31] or abnormal dispersion behavious[14]). This is how we related the phase matching ability with the birefringence, although the refractive index of many optical materials depends on the intensity of the light when using the high energy light.

The calculated imaginary parts of the dielectric function for the AX_2MQ_6 crystals for photon energy up to 10eV are shown in SI. The refractive index are calculated and then resolved into two components, the in-plane component n_{xy} *i.e.* ordinary refractive index n_o is the average over the x and the y directions and the z componet *i.e.* extraodinary refractive index which is perpendicular to n_{xy}. To relate the phase matching abilities with linear optical properties, we calculated $\Delta n_{2\nu}$,Δn_0 and $n_e^{\nu} - n_o^{2\nu}$ and put them in Table.3.

Calculation of the birefringence in AX_2MQ_6 structures reveal the following regularitise: The birefringece value increase with increasing ion radius. We use the pauling ion radius[32]. If the change of the absolute value of delta n_0 is considered, it is seen from Fig.2 that in substituting for the filling cations (Ba $\rightarrow$ Cs) or for the framework (Si $\rightarrow$ Ge $\rightarrow$ Sn),(S $\rightarrow$ Se) anions in AX_2MQ_6 compounds, the birefringence value positive correlated with ion radius.

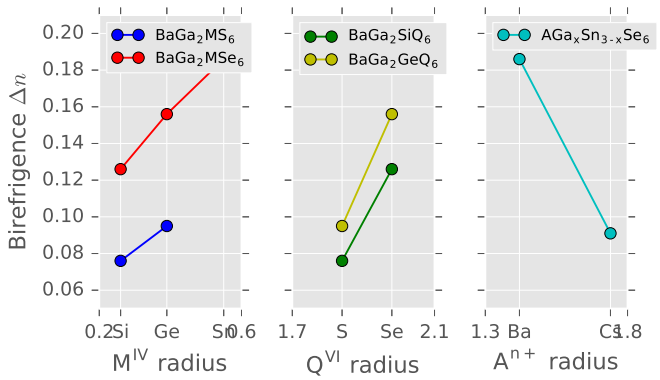

Figure 2 The dependence of the birefringence of AX_2MQ_6 crystals on the pauling ion radii R

iv. Distinct anisotropy of AX_2MQ_6 and $AX_4M_5Q_{12}$

In transparent materials, refractive index is proportional to the square root of the electronic polarization. The latter is in turn proportional to the polarizabilities of the ions in the crystal and also the local electric field. Densely packed arrays of highly polarizable group alignment result in large refractive indices. The different direction of anisotropic groups lead to the different refractive indices of ordinary and extraordinary optical planes which is the reason of birefringence of crystals.

Both AX_2MQ_6 and $AX_4M_5Q_{12}$ belong to space group R3(No.146) and can be derived from zinc-blende struture that why we call these structure diamond-like framework(DLF) structure. From the angle of view perpendicular to c axis(the C_3 rotation axis), the crystal can be cut to layers constructed by polarized tetrahedrons. The layers viewed from c axis(Fig.3a, Fig.3c) are different for AX_2MQ_6 and $AX_4M_5Q_{12}$ but both can be regarded as

Table 3 Structure and optical properties of AX_2MQ_6 crystals.

Compounds	dihedral angle θ	Δn^0	Δn^{2v}	$\lvert\chi^{(2)}_{max}\rvert$	$n_e^v - n_o^{2v}$	band gap (eV)
$BaGa_2SiS_6$	4.501	0.076	0.083	39.382	+	2.823
$BaGa_2SiSe_6$	5.410	0.126	0.143	76.014	+	2.166
$BaGa_2GeS_6$	5.041	0.095	0.106	45.417	+	2.358
$BaGa_2GeSe_6$	5.771	0.156	0.197	102.139	+	1.507
$BaGa_2SnSe_6$	6.091	0.186	0.269	159.946	+	1.412
$CsSi_2GaS_6$	-1.05	0.006	0.008	38.518	-	3.078
$CsSi_2GaSe_6$	0.892	0.025	0.029	67.926	-	2.351
$CsGe_2GaS_6$	0.713	0.027	0.033	51.340	-	2.536
$CsGe_2GaSe_6$	2.480	0.061	0.085	110.475	-	1.648
$CsSn_2GaSe_6$	4.507	0.091	0.153	125.767	+	1.332

three tetrahedra bundles (Fig.3b, Fig.3d) tiled layers.

As what mentioned in electronic structure subsection i, the Q^{2-} contribute most to the transition from occupied states to unoccupied states. And compare with the zinc-blende structure whose Q^{2-} are sp^3 hybridization and four coordinate to cations, the Q^{2-} ions are two coordinate and three coordinate in AX_2MQ_6 and $AX_4M_5Q_{12}$ respectively.

In AX_2MQ_6, the Q^{2-} is sp^3 hybridization and two coordinate which lead to the appearence of two pairs of lone pairs in each Q atoms. The location of the lone pairs ought to be the bond of zinc-blende structure. However, replacement of atoms and structure distortion make the lone pairs deviate from the origin location.

We attribute the different birefringence to the acentricity of Q^{2-} *i.e.* the existent of lone pairs and their location devidation. Because Q^{2-} plays the decisive role in optical properties and displays remarkable anisotropy. Nevertheless, the location of lone pairs is hard to be quantification to reveal the quantitative relation between birefringence and structure. We therefore define a geometric feature the dihedral angle between tetrahedrons' underside and xy-plane. As show in Fig.3b and Fig.3d, the undersides of tetrahedrons have been labeled as α, β and γ, and the xy-plane was labeled as Σ. We defined the quantifiable dihedral angle to be θ:

$$\theta = \frac{\measuredangle(\alpha,\Sigma) + \measuredangle(\beta,\Sigma) + \measuredangle(\gamma,\Sigma)}{3} \tag{7}$$

This geometirc feature can be measured easily by using structrue viewer softwares such as VESTA[33] (as shown in Fig.4) after getting the crystal structure.

In $AX_4M_5Q_{12}$, the Q^{2-} have same hybridization but three coordinate which lead to the single lone pairs. The location of the lone pairs also deviated from the origin zinc-blende bond.

The birefringence of $AX_4M_5Q_{12}$ crystals are extremely low <0.01 in transmission frequencies. But the birefringence of AX_2MQ_6 are variable in a wide range from 0.06($CsSi_2GaS_6$) to 0.186($BaGa_2SnSe_6$). The low birefringence of $AX_4M_5Q_{12}$ is result partly from small radiu Cd atoms as we interperate from the relation of ion radius and birefringence.

However, the anisotroy of the crystal are contributed mostly from the acentricity of Q^{2-} which can be related to its lone paris positional deviation. As shown in Fig.3a and Fig.3c, the bundle of tetrahedrons are viewed from top to bottom along the c axis. We can find that for $BaGa_2SnSe_6$ the lone pairs above the Q atoms are centralize to the C_{3v} axis while the small birefringence compounds $CsGaSn_2Se_6$ and $CsCd_4Ga_5Se_{12}$ have the lone pairs locate at the direction where the original bonds locate of zinc-blende strucure. Using the parameter we definded to quantification the lone pairs' positional deviation, we find good correlation between birefringence and structure parameter as shown in Fig.5 which explains birefringen difference in all AX_2MQ_6 and $AX_4M_5Q_{12}$ struture.

Taking the biggist birefringence compound $BaGa_2Snse_6$ as example, its large birefringence attribute to: 1. the large radius of Sn and Se atoms; 2. the strong acentricity i.e. lone pairs positional deviation which comes from the distortion between tetrahadrons. As mentioned before, AX_2MQ_6 have more sparse network connection between tetrahedrons, therefore more freedom for atoms off-centeterd movement. However, the dense tetrahedral network of $AX_4M_5Q_{12}$ makes atoms hard to deviate from central location and stay the isotropy as zinc-blende structure.

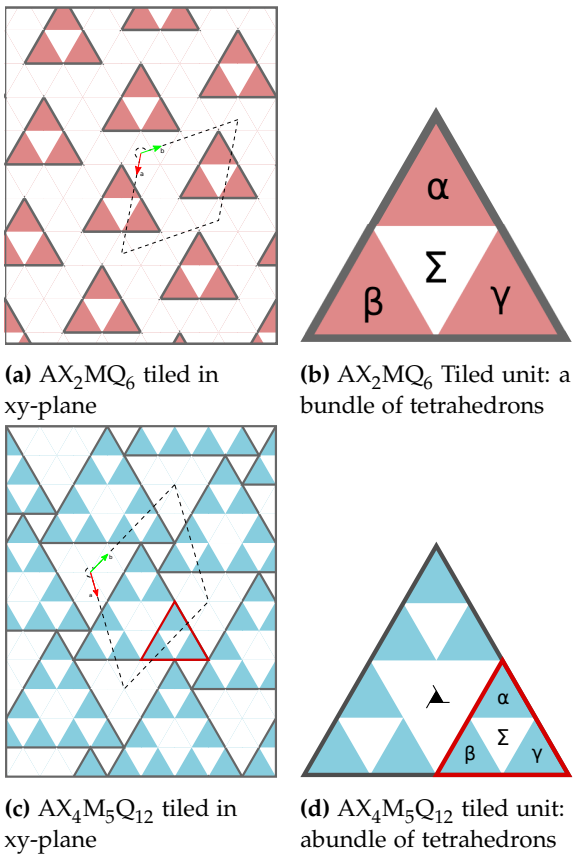

(a) AX_2MQ_6 tiled in xy-plane

(b) AX_2MQ_6 Tiled unit: a bundle of tetrahedrons

(c) $AX_4M_5Q_{12}$ tiled in xy-plane

(d) $AX_4M_5Q_{12}$ tiled unit: abundle of tetrahedrons

Figure 3 Layers structure viewed from c-axis and its constructive units

V. Summary

Linear optical properties especially the anisotropy of R3 space group diamond-like framework crystal AX_2MQ_6 and $AX_4M_5Q_{12}$ was done with first-principles calculation.

Both AX_2MQ_6 and $AX_4M_5Q_{12}$ are partial occupation compounds. The models of a resonable configuration which can accurately reflect the material properties is hard to be chosen. We use SOD program to enumerate all possible configurations in a $1 \times 1 \times 1$ hexagnal convetional cell and confirm that the $P3_1$(No.144) and $P3_2$(No.145) are resonable configuration.

We also investigate the structural and electronic mechanisms of the anisotropic optical properties in these materials. On the one hand, we reveal the correlation of birefringence and framework ion radius that the birefringence is increase with bigger framework ion radius. On the other hand, geometric parameter the dihedral angles between xy-plane and tetrahedrons' underside was defined to quantificat the acentricity factor of anisotropy of crystal. The birefrigence and dihedral angles between xy-plane and tetrahedrons' underside are well positive correlation. These two factors combined to explain the different birefringence of AXM_2Q_6 and $AX_4M_5Q_{12}$ from <0.001 to 0.186. And the phase matchability of these crystal can be explained with these birefringence data. For the existent of geometric-property relationship, it is possible to control the anisotropy of crystal by adjusting the geometric parameter.

Meanwhile, by comparing birefringence we find the hypothetical structures CsQ_2GaM_6 (Q=Ge, Si; M=Se, S) are unlikely to reach phase matching condition. We believe that the evaluation of structure-property correlation in our work has implications in the exploration of new IR-NLO crystals with good performance.

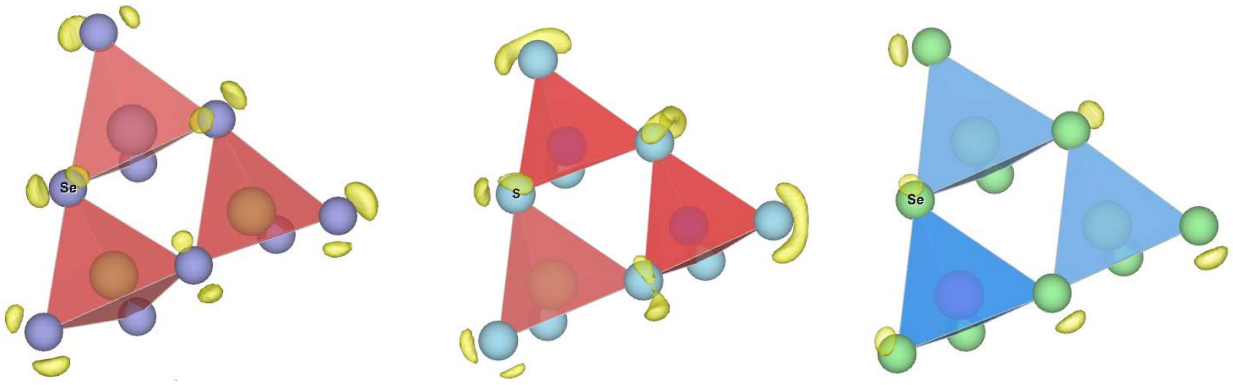

(a) ELF of $BaGa_2SnSe_6$ **(b)** ELF of $CsSi_2GaS_6$ **(c)** ELF of $CsCd_4Sn_5Se_6$

Figure 4 ELF of $BaGa_2SnSe_6$, $CsSi_2GaS_6$ and $CsCd_4Ga_5Se_{12}$

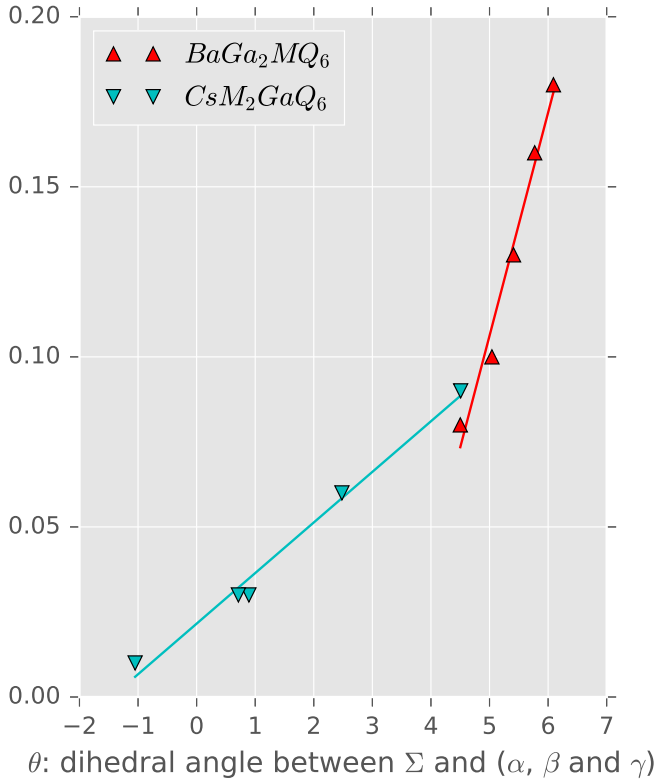

Figure 5 Dependence of birefringence on defined dihedral angle θ

References

[1] Z. Lin, X. Jiang, L. Kang, P. Gong, S. Luo and M.-H. Lee, *Journal of Physics D: Applied Physics*, 2014, **47**, 253001.

[2] N. Goryunova, L. Zlatkin and E. Ivanov, *Journal of Physics and Chemistry of Solids*, 1970, **31**, 2557 – 2561.

[3] Y. Shen, *Principles of nonlinear optics*, Wiley-Interscience,New York, NY, USA, 1984.

[4] R. W. Boyd, *Nonlinear Optics (Third Edition)*, Academic Press, Burlington, Third Edition edn, 2008, pp. 69 – 133.

[5] X. Lin, G. Zhang and N. Ye, *Crystal Growth and Design*, 2008, 7–10.

[6] H. Lin, L. Chen, L.-J. Zhou and L.-M. Wu, *Journal of the American Chemical Society*, 2013, **135**, 12914–12921.

[7] X. Li, C. Li, P. Gong, Z. Lin, J. Yao and Y. Wu, *Journal of Materials Chemistry C*, 2015, **3**, 10998–11004.

[8] W. Yin, K. Feng, W. Hao, J. Yao and Y. Wu, *Inorganic Chemistry*, 2012, **51**, 5839–43.

[9] D. Zhao, W. D. Cheng, H. Zhang, S. P. Huang, Z. Xie, W. L. Zhang and S. L. Yang, *Inorganic Chemistry*, 2009, **48**, 6623–6629.

[10] R. E. R. E. Newnham, *Properties of materials : anisotropy, symmetry, structure*, Oxford University Press, 2005, p. 378.

[11] M. A. M. Fox, *Optical properties of solids*, Oxford University Press, 2001, p. 305.

[12] D. S. Chemla, *Physical Review Letters*, 1971, **26**, 1441–1444.

[13] F. Qin and R. Li, *Journal of Crystal Growth*, 2011, **318**, 642–644.

[14] X. Jiang, S. Luo, L. Kang, P. Gong, H. Huang, S. Wang, Z. Lin and C. Chen, *ACS Photonics*, 2015, **2**, 1183–1191.

[15] Q. Bian, Z. Yang, L. Dong, S. Pan, H. Zhang, H. Wu, H. Yu, W. Zhao and Q. Jing, *Journal of Physical Chemistry C*, 2014, **118**, 25651–25657.

[16] A. Savin, R. Nesper, S. Wengert and T. F. Fässler, *Angewandte Chemie International Edition in English*, 1997, **36**, 1808–1832.

[17] R. Grau-Crespo, S. Hamad, C. R. A. Catlow and N. H. de Leeuw, *Journal of Physics: Condensed Matter*, 2007, **19**, 256201.

[18] P. Giannozzi, S. Baroni, N. Bonini, M. Calandra, R. Car, C. Cavazzoni, D. Ceresoli, G. L. Chiarotti, M. Cococcioni, I. Dabo, A. Dal Corso, S. de Gironcoli, S. Fabris, G. Fratesi, R. Gebauer, U. Gerstmann, C. Gougoussis, A. Kokalj, M. Lazzeri, L. Martin-Samos, N. Marzari, F. Mauri, R. Mazzarello, S. Paolini, A. Pasquarello, L. Paulatto, C. Sbraccia, S. Scandolo, G. Sclauzero, A. P. Seitsonen, A. Smogunov, P. Umari and R. M. Wentzcovitch, *Journal of physics. Condensed matter : an Institute of Physics journal*, 2009, **21**, 395502.

[19] G. Kresse, *Physical Review B*, 1996, **54**, 11169–11186.

[20] G. I. Csonka, J. P. Perdew, A. Ruzsinszky, P. H. T. Philipsen, S. Leb??gue, J. Paier, O. A. Vydrov and J. G. ??ngy??n, *Physical Review B - Condensed Matter and Materials Physics*, 2009, **79**, 1–14.

[21] H. J. Monkhorst and J. D. Pack, *Physical Review B*, 1976, **13**, 5188–5192.

[22] G. Kresse and D. Joubert, *Physical Review B*, 1999, **59**, 1758–1775.

[23] M. Gajdoš, K. Hummer, G. Kresse, J. Furthmüller and F. Bechstedt, *Physical Review B - Condensed Matter and Materials Physics*, 2006, **73**, 1–9.

[24] N. Wiser, *Physical Review*, 1963, **129**, 62–69.

[25] G. Onida, L. Reining and A. Rubio, *Reviews of Modern Physics*, 2002, **74**, 601–659.

[26] C. Aversa and J. E. Sipe, *Physical Review B*, 1995, **52**, 14636–14645.

[27] S. N. Rashkeev, W. R. L. Lambrecht and B. Segall, *Physical Review B*, 1998, **57**, 3905–3919.

[28] N. W. Ashcroft and N. D. Mermin, *Solid state physics*, Holt, Rinehart and Winston, 1976, p. 826.

[29] S. K. Kurtz, *Journal of Applied Physics*, 1968, **39**, 3798.

[30] I. Chung and M. G. Kanatzidis, *Chemistry of Materials*, 2014, **26**, 849–869.

[31] R. E. Nettleton, *Journal of computational physics*, 1971, **603405**, 603–605.

[32] R. D. Shannon and IUCr, *Acta Crystallographica Section A*, 1976, **32**, 751–767.

[33] K. Momma and F. Izumi, *Journal of Applied Crystallography*, 2011, **44**, 1272–1276.

VI. SI

$BaGa_2SiS_6$	a	c	V
exp	9.5544(2)	8.6498(4)	683.82(2)
PBEsol	9.462	8.556	663.318
PBE	9.710	8.716	711.641
pz-LDA	9.355	8.484	643.081
$BaGa_2SiSe_6$	a	c	V
exp	9.967(1)	9.047(2)	778.3(2)
PBEsol	9.925	9.006	768.225
PBE	10.188	9.210	827.810
pz-LDA	9.799	8.959	744.981
$BaGa_2GeS_6$	a	c	V
exp	9.6020(1)	8.6889(2)	693.78(2)
PBEsol	9.502	8.623	674.275
PBE	9.740	8.840	726.317
pz-LDA	9.375	8.608	655.176
$BaGa_2GeSe_6$	a	c	V
exp	10.008(1)	9.090(2)	788.4(2)
PBEsol	9.949	9.093	779.410
PBE	10.208	9.377	846.335
pz-LDA	9.803	9.097	757.133
$BaGa_2SnSe_6$	a	c	V
exp	10.1449(14)	9.2490(18)	824.4
PBEsol	10.054	9.326	816.477
PBE	10.315	9.639	888.085
pz-LDA	9.908	9.334	793.519

Table 4 Lattice parameters compare with experiment data

Models		
Crystal	Configuration	Energy (Ry)
$BaGa_2SiS_6$	No.143	-1750.217
	No.144	(-)0.020
	No.145	(-)0.044
$BaGa_2SiSe_6$	No.143	-1836.936
	No.144	(-)0.020
	No.145	(-)0.036
$BaGa_2GeS_6$	No.143	-2348.947
	No.144	(-)0.031
	No.145	(-)0.014
$BaGa_2GeSe_6$	No.143	-2435.772
	No.144	(-)0.023
	No.145	(-)0.012
$BaGa_2SnSe_6$	No.143	-2249.162
	No.144	(-)0.017
	No.145	(-)0.004

Table 5 Ground state energy of different configurations